Early Age Behavior of Wind Turbine Gravity Foundations

J. Modu, J. F. Georgin, L. Briançon, E. Antoinet

Abstract—Wind turbine gravity foundations are designed to resist overturning failure through gravitational forces resulting from their masses. Owing to the relatively high volume of the cementitious material present, the foundations tend to suffer thermal strains and internal cracking due to high temperatures and temperature gradients depending on factors such as geometry, mix design and level of restraint. This is a result of a fully coupled mechanism commonly known as THMC (Thermo- Hygro - Mechanical - Chemical) coupling whose kinetics peak during the early age of concrete. The focus of this paper is therefore to present and offer a discussion on the temperature and humidity evolutions occurring in mass pours such as wind turbine gravity foundations based on sensor results obtained from the monitoring of an actual wind turbine foundation. To offer prediction of the evolutions, the formulation of a 3D Thermal-Hydro-Chemical (THC) model that is mainly derived from classical fundamental physical laws is also presented and discussed. The THC model can be mathematically fully coupled in Finite Element analyses. In the current study, COMSOL Multi-physics software was used to simulate the 3D THC coupling that occurred in the monitored wind turbine foundation to predict the temperature evolution at five different points within the foundation from time of casting.

Keywords—Early age behavior, reinforced concrete, THC 3D models, wind turbines.

I. INTRODUCTION

THE demand for onshore wind energy continues to grow along with the increased need for sustainable energy. In Europe, the wind energy market is envisioned to evolve between 2020 and 2030 by retrofitting existing parks. Therefore, the current research work constitutes a part of a project known as FEDRE Project FUI 25 that seeks to allow reuse of the existing wind turbine foundations. The solution shall be applicable during the repowering phase whereby the turbines have either reached the end of their service lives or need to be replaced with more powerful turbines for increased electricity production.

The general approach adopted in this research work is firstly to fully understand the behavior of an existing wind turbine foundation (Fig. 1). To do so, it was found imperative to investigate each phase during the course of its life; from casting to deconstruction. The initial phase of the concrete from casting up to 28 days during which the concrete attains its strength is what is commonly known as the early age of concrete. The early age study therefore constitutes the initial phase of the research work and shall be the focus of this paper.

Fig. 1 Monitoring of a 20 m diameter wind turbine foundation at Les Pierrots, France

During the casting and curing phase, the complexity of concrete as a porous media reveals itself through the chemical processes occurring when the cement phase or its equivalent chemically interacts with water causing it to harden. This triggered the interest of researchers such as H.F.W. Taylor in [1] to conduct research on the chemistry of cement. The author's insightful works have been the basis for the understanding of cement properties. Following their work, numerous researchers have proposed models to predict the hydration kinetics of concrete. Works by [2] and [3] propose a simplified and generalized approach for predicting the hydration kinetics of slag-blended cements following earlier research works of [4]-[6].

Due to scale effect, some models derived from laboratory experiments on small specimens may not be directly applicable to massive structures. On the other hand, some hydration models such as DUCOM, CEMHYD3D and HYMOSTRUC offer realistic evolutions but are not suitable for large structures due to their long computing time [2]. This necessitates independent studies on massive structures to propose models suitable for their designs.

According to [7], mass concrete is any volume of structural concrete that due to the elevated temperatures caused by heat produced during hydration can lead to undesirable thermal stresses, cracking, deleterious chemical reactions, or reduction in the long-term strength. Due to the exothermic nature of the chemical reaction during hydration, the temperature in mass concrete may elevate to temperatures that are detrimental to the

J. O. Modu is with the Univ. Lyon, INSA-Lyon, GEOMAS, F-69621, Villeurbanne, France (corresponding author, phone: +33787598782; e-mail: janetoswald.modu@insa-lyon.fr).

J. F. Georgin and L. Briançon are with the Univ. Lyon, INSA-Lyon, GEOMAS, F-69621, Villeurbanne, France (e-mail: jean-francois.georgin@insa-lyon.fr, laurent.briancon@insa-lyon.fr).

E. Antoinet is with ANTEA Group, 45166 OLIVET, France (e-mail: eric.antoinet@anteagroup.com).

World Academy of Science, Engineering and Technology
International Journal of Civil and Environmental Engineering
Vol:16, No:3, 2022

durability and integrity of the structure. Above 70 ° C, the concrete is at risk of forming delayed ettringite which is characterized by its expansive behavior in hardened concrete. The presence of ettringite in hardened concrete subsequently leaves the concrete at risk of internal cracking [8]. Also, concerning moisture necessary for hydration, studies have reported that below relative humidity of 80% in portland cement, the hydration reaction almost completely stops [9], [10]. However, other factors also play a role in the formation of delayed ettringite [11].

In addition, massive structures suffer thermal strains due to high thermal gradients between the core of the structure and its surfaces depending on curing conditions. During temperature increase, the core of the structure tends to expand and due to internal restraint, compressive stress is developed in the interior and tensile stress on the surfaces [12]. To quantify the risk level of cracking, factors such as level of restraint need to be taken into account [13].

With an appreciation of the numerous studies made so far on the coupled mechanisms of early age concrete as in [14]-[16], [18] this paper aims to provide actual data of the temperature and humidity evolutions in a 20 m diameter wind turbine foundation while offering a formulation of a predictive model for its kinetics that maintains underlying fundamental principles already formulated in previous works. The mathematical models are presented in such a way to allow implementation on Finite element models such as COMSOL Multiphysics for simulation of early age behaviour of massive structures. The properties of the reference foundation shown in Fig. 1 shall be used to illustrate the applicability of the model.

II. 3D THC Model Numerical Implementation

The reinforced concrete wind turbine foundation was modelled in 3D mainly based on the properties of the real foundation. The numerically implemented foundation comprised of about 900 tons of concrete with cement of type CEM 3 underlain by a 5.5 m deep soil layer. A reduced depth introduced numerically at which no boundary effect in temperature could be detected (Fig. 2). Only half of the foundation is shown.
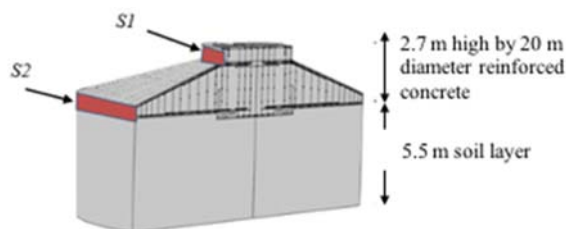
Fig. 2 Numerical representation of a wind turbine gravity foundation

The curing conditions were introduced into the numerical model through such formwork placement on the vertical portions of the foundation as shown in Fig. 2 denoted by S1 and S2. The wooden formworks were not geometrically modelled; however, they were taken into account by introducing physical properties that would allow simulation of heat transfer from

concrete through the formworks and into the surrounding air. The removal of formwork was on day 2 after commencement of casting in which flux conditions after this period were those with air.

The built-in Partial Differential Equations (PDE) on COMSOL are satisfied by introducing appropriate source terms, initial values and boundary conditions (Dirichlet or Neumann type) assigned for each individual mechanism within the early age simulation.

Generally, the partial differential equations on COMSOL Multiphysics are in the form as given in (1). Reference [17] can be referred to.

$$e_a \frac{\delta^2 \mathbf{v}}{\delta t^2} + d_a \frac{\delta \mathbf{v}}{\delta t} + \nabla.(-c\nabla\mathbf{v} - \alpha\mathbf{v} + \gamma) + \beta.\nabla\mathbf{v} + a\mathbf{v} = f \quad (1)$$

$$\nabla = [\frac{\delta}{\delta x}, \frac{\delta}{\delta y}, \frac{\delta}{\delta z}]$$

where $\mathbf{v}$ is the variable to be solved for, e_a is mass coefficient, d_a is damping /mass coefficient, c is diffusion coefficient, α is conservation flux convection coefficient, γ is conservation flux source, β is convection coefficient, a is absorption coefficient, f is the source term and ∇ is the Laplace operator.

For simulation of heat transfer, the following general equation defined on COMSOL is used.

$$\rho C_p \frac{\delta T}{\delta t} + \rho C_p \mathbf{u}. \nabla T + \nabla. \mathbf{q} = Q \quad (2)$$
$$\mathbf{q} = -k\nabla \mathbf{T}$$

where ρ is the density, C_p is the heat capacity at constant pressure, T is the variable to be solved for in this case temperature, $\mathbf{u}$ is the deformation, k is the thermal conductivity and Q is the source term.

For a complete THC simulation, five mechanisms are defined using independent *nodes* (the term *nodes* as described on COMSOL) but shall be referred to as *sub-models* in this paper. The following sub-models are introduced; 1) Hydration model 2) Porosity model 3) Transfer of liquid water model 4) Transfer of vapor model 5) Transfer of dry air model 6) Heat transfer model. Within each sub-model, dependence on the other models is incorporated. The fundamentals on the mass transfer models are specifically based on the porous media approach by [5] and the generalized hydration model by [2] and [3]. Formulation of the five aforementioned mechanisms shall be discussed.

A. Hydration Model

The cement hydration is based on the definition of the degree of hydration, α. It corresponds to the fraction of initially available anhydrous cement, m_c that has dissolved in the porous solution and is assumed to be hydrated, $m_c^{disolved}$ (3).

$$m_c^{disolved} = \alpha \, m_c \quad (3)$$

The model that governs the hydration kinetics comes from the work of [2], [3] and [12] in which (4) is used.

World Academy of Science, Engineering and Technology
International Journal of Civil and Environmental Engineering
Vol:16, No:3, 2022

$$\dot{\alpha} = k \, \Pi \, A \, exp\left(-\frac{Ea}{T}\right) \qquad (4)$$

where the coefficient of accessibility to water, $\Pi = exp\left[-B\left(\frac{r_m}{r_k}\right)^n\right]$, A is the coefficient of chemical activation, r_m the accessibility radius, Ea the activation energy and T the internal temperature of the concrete. k, r_k, n and B are calibration constants that can be attained by performing adiabatic calorimeter tests as performed by [3]. The ratio E_a/R for concrete normally ranges between 3000 and 8000 K and can be experimentally determined [16].

It is shown in the hydration model in (4), the integration of the hygro- and thermal components of the THC coupling through the coefficient of accessibility to water Π and the internal temperature T respectively.

During the hydration process, the microstructure is constantly changing according to (5) defined by a continuously changing porosity, ϕ. Where, β_{chat} is the Le chatelier constant (accounts for volume reduction), d_c the cement density, d_w liquid water density, m_c the cement mass and γ_c the amount of water needed to chemically react with the total quantity of cement. The microstructure development is shown to depend on the rate of hydration, $\dot{\alpha}$.

$$\dot{\phi} = \dot{\alpha}\left[1 - \beta_{chat}\left(1 + \gamma_c \frac{d_c}{d_w}\right)\right]\frac{m_c}{d_c} \qquad (5)$$

B. Thermal Model

The thermal transfer mechanism within the foundation is modeled based on the following heat equation in which the dependent variable is temperature, T [K].

$$\rho \, C_p \, \frac{dT}{dt} + div\left(-\lambda_T \, grad(T)\right) = \frac{dQ_1}{dt} + \frac{dQ_2}{dt} \qquad (6)$$

where ρ (kg/m^3) is the concrete density, C_p (J/(kg·K)) is the heat capacity at constant pressure and λ_T (W/(m·K)) is the thermal conductivity. In the simulation, these parameters are considered constant, however, they vary depending on the temperature [4], [20].

The heat source, Q_1 (W/m^3) is the heat exerted by the hydration reactants during the hydration process. According to [16], assuming a constant theoretical heat of hydration $Q_{\xi,i}$, the rate of heat source Q_1 can be defined as;

$$\frac{dQ_1}{dt} = \dot{\alpha} \, m \, Q_\xi \qquad (7)$$

The rate of the amount of energy required to change the evaporable water from liquid to vapor state is as given in (8);

$$\frac{dQ_2}{dt} = -\frac{dm_{\ell \to v}}{dt} L_{\ell \to v} \qquad (8)$$

where $m_{\ell \to v}$ is the quantity of water transformed from liquid phase to vapor phase during heating and $L_{\ell \to v}$, the heat of vaporization.

In the thermal model, the coupling with the chemical and hygro- mechanisms is implemented through heat sources Q_1

and Q_2 where hydration and mass transfer terms α and $m_{\ell \to v}$ respectively are used.

C. Mass Transfer Model

The fluid within the concrete occupies the porous volume assumed to be connected. The three main fluid phases are identified by their mass per unit volume of porous material, m_i using (9) to (11) where subscript *i* denotes liquid (l), vapor (v) and air (a) phases of which their main dependent variables in the simulation are; saturation, S relative humidity, h and air pressure, p_a respectively. The density of liquid water, ρ_ℓ is assumed constant while those of vapor (ρ_v) and dry air (ρ_a) are temperature dependent. According to the density formula given in [21], the effect of the water density variation with temperature can be negligible in the hydration process.

$$m_\ell = \rho_\ell \, \phi \, S \qquad (9)$$

$$m_v = \rho_v \, \phi \, (1 - S) \qquad (10)$$

$$m_a = \rho_a \, \phi \, (1 - S) \qquad (11)$$

The transport mechanisms for each phase are formulated by considering separate diffusion equations since the driving forces are unique to each mechanism. Conservation equations used for the liquid, vapor and air phases are as given in (12) to (14) respectively.

$$\frac{\partial m_\ell}{\partial t} + div(w_\ell) = -\frac{\partial m_{\ell \to v}}{\partial t} - \frac{\partial m_{\ell \to \xi}}{\partial t} \qquad (12)$$

$$\frac{\partial m_v}{\partial t} + div(w_v) = \frac{\partial m_{\ell \to v}}{\partial t} \qquad (13)$$

$$\frac{\partial m_a}{\partial t} + div(w_a) = 0 \qquad (14)$$

where $m_{\ell \to \xi}$ is the quantity of water consumed by cement hydration.

The flows of the three phases (w_i) making up the fluid are governed by the known transfer laws; Darcy's law and Fick's law. Darcy's law is used for liquid transfer as given in (15).

$$w_\ell = -\rho_\ell \frac{K_\ell^{eff}}{\eta_\ell} \nabla(p_\ell) \qquad (15)$$

where p_ℓ is liquid pressure, K_ℓ^{eff} the effective liquid water permeability of the porous medium, η_ℓ the viscosity of water, and ρ_ℓ the liquid density.

For the flow in vapor and air state, the Fick's law is included to define the diffusive characteristic (16) and (17).

$$w_v = -D_{eff}\nabla\rho_v - \rho_v \frac{K_v^{eff}}{\eta_g} \nabla p_g \qquad (16)$$

$$w_a = -D_{eff}\nabla\rho_a - \rho_a \frac{K_v^{eff}}{\eta_g} \nabla p_g \qquad (17)$$

with D_{eff} the effective diffusion coefficient of vapor/dry air in humid air, K_v^{eff} the effective relative vapor permeability of the

World Academy of Science, Engineering and Technology
International Journal of Civil and Environmental Engineering
Vol:16, No:3, 2022

porous medium and p_g the pressure of gaseous mix (humid air).

The amount of liquid water contained within the pores depends on two things; the total porosity (available pore volume) and the pore size distribution. Indeed, in the pore network, the pressure of liquid water, the vapor pressure and the surface tension are in equilibrium. The pressure difference between the liquid phase and the vapor phase is governed by the following Kelvin Laplace relation.

$$p_g - p_\ell = -\rho_\ell \frac{RT}{M_l} ln(h) \qquad (18)$$

with $p_g = p_v + p_a$ law of partial pressure, R a perfect gas constant, T temperature and M_l molar mass of liquid water. h is the relative humidity in ratio of vapor pressure, p_v and saturated vapor pressure, p_{vsat}. As a result, a meniscus with radius R_m and surface tension γ is formed described by (19).

$$p_g - p_\ell = \frac{2\gamma}{R_m} \qquad (19)$$

with $p_g = p_v + p_a$ law of partial pressure, R a perfect gas constant, T temperature and M_l molar mass of liquid water. h is the relative humidity in ratio of vapor pressure, p_v and saturated vapor pressure, p_{vsat}. As a result, a meniscus with radius R_m and surface tension γ is formed described by (19).

(a)   (b)

(c)
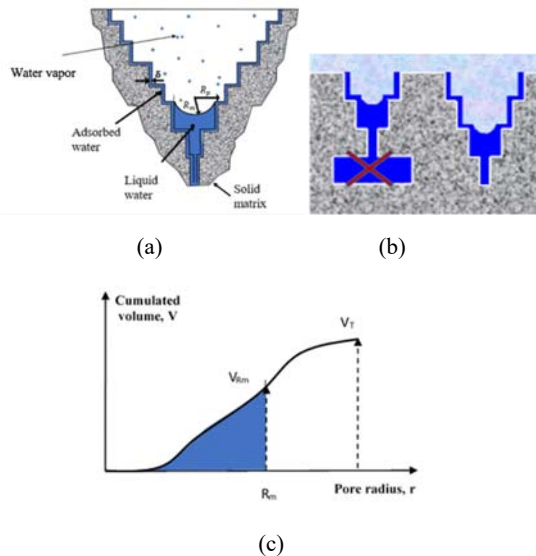
Fig. 3 Porous medium a) Liquid, vapor and air masses at equilibrium in pore spaces b) Considered pore structure sequence c) Cumulated pore volume at each time, t

Thus, the degree of saturation can be estimated according to the degree of humidity with a desorption isotherm relationship as given in (20) and (21).

$$S = \frac{V_{R_m}}{V_T} = f(h) \qquad (20)$$

Note that the desorption isotherm can be evaluated experimentally when the microstructure of the material is stabilized. At an early age, the use of a model to describe the

isotherm as a function of the degree of hydration is necessary. Equation (21) provides the saturation - humidity relationship dependent on the hydration level where m_s and n_s are empirical constants. It is derived as an exponential form based on (18) and (19) and the pore structure as shown in Fig. 3.

$$S = \left\{ 1 - exp \left[-m_s * \frac{2\gamma M_l}{\rho_\ell RT\, ln(h)} * exp(n_s \alpha) \right] \right\} \qquad (21)$$

D. Boundary Conditions

The equation to simulate surface heat flux q_0 is as given in (22) where h_{eq} is the equivalent heat transfer coefficient, T_{ext} is the external temperature and T the evolving surface temperature.

$$q_o = h_{eq}(T_{ext} - \text{T}) \qquad (22)$$

h_{eq} accounts for both convective and radiative exchanges and in the presence of formwork, the heat transfer through conduction term is included ($\frac{e}{\lambda}$ term).

$$\frac{1}{heq} = \frac{1}{h_{rad}+h_{air}} + \frac{e}{\lambda} \qquad (23)$$

where h_{rad} is the radiative exchange coefficient, h_{air} is the convective exchange coefficient in air which accounts for wind speed. λ is the thermal conductivity of formwork and e is the formwork thickness.

To simulate liquid water and vapor fluxes, (24) and (25) are used. E_l and E_V are the coefficients of hydric liquid and vapor emissivity respectively, P_{sv} and P_{svext} the saturated vapor pressures dependent on internal and external foundation temperatures respectively.

$$Flux_l = -\Phi S E_l(P_{sv} - h_{ext}.P_{svext}) \qquad (24)$$

$$Flux_v = -\Phi(1-S)E_V(hP_{sv} - h_{ext}P_{svext}) \qquad (25)$$

In the case of dry air, a Dirichlet boundary condition is defined in which the atmospheric pressure of 101325 Pa is assigned.

III. EARLY AGE MONITORING OF IN-SITU FOUNDATION

In addition to the formulation of a predictive model for the kinetics in gravity foundations, it was vital to monitor the temperature and humidity evolutions of an actual wind turbine gravity foundation during the casting and curing period (Fig. 4 and 5). This is to acquire knowledge on the maximum temperature and temperature gradient achieved within the foundation and also to offer validation to the 3D THC model.

Fig. 4 Casting of a wind turbine foundation at Les Pierrots, France

World Academy of Science, Engineering and Technology
International Journal of Civil and Environmental Engineering
Vol:16, No:3, 2022
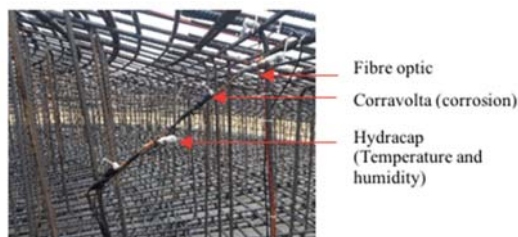
Fig. 5 Temperature and humidity monitoring of a wind turbine foundation at Les Pierrots, France

The schematic of a section of the foundation shown in Fig. 6 presents the locations of *hydracap* sensors known to take measurements of temperature and relative humidity at a particular point and a fibre optic to obtain temperature measurements along its length at every 2.6 mm. In the *hydracap* sensor, a unique capacitive sensor element is used to measure relative humidity while a band-gap sensor is used to measure the temperature. The fibre optic uses a rayleigh back scattering technique which adopts the principle of light propagation.

In the foundation, six *hydracap* sensors were placed (denoted as T0 to T5) and five of the six sensors produced measurements. No measurements were obtained from sensor T2 probably due to a cut on the sensor's cable as a result of the site's harsh environment.
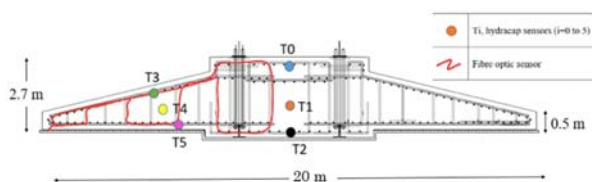
Fig. 6 Temperature and humidity sensor positions

A. Temperature

A plot of temperature evolution attained numerically (T00 to T55) and from sensor measurements (T0 to T5) is presented on Fig. 7. It is evident through sensor T1 placed at the core of the foundation that the foundation achieved a maximum temperature of about 65 °C 58 hours (2.4 days) after pouring. The temperature value is within the maximum threshold of about 70 °C to avoid cracking. However, as it is not too far from the threshold, it would be advantageous to conduct a study of core samples of an actual wind turbine during its deconstruction to observe presence or absence of ettringite. In Fig. 7, time t= 0 hours is the time at which concrete pouring commenced. However, the first data point provided for each sensor is at 6 hours after casting began when nearly all sensors were considered fully immersed within the concrete. Between 0 to 6 hours, some sensors were fully immersed before others resulting to different initial times. However, since the exact time at which each sensor was immersed was not recorded, Fig. 7 assumes an initial for all sensors as the time at which casting commenced.

A maximum temperature differential of about 35 °C four days after casting is determined from sensor T1 at the core and sensors T0 and T3 near the surfaces. Other factors such as level

of restraint which influence the cracking potential need to be determined to evaluate the risk of cracking.

Upon comparing the model to the sensor measurements, a good agreement can be observed for all the five sensors. However, while the trend of the evolution is well predicted, the accuracy at some points especially at the surfaces is compromised. A maximum error of 11 % is obtained near the surface of the foundation (at position T00) at which the maximum temperature occurred 20 hours earlier relative to the time of maximum temperature provided by the sensor at this location (at position T0). Also, the rate of temperature increase is noticeably higher at this point which may be due to an over-prediction of the hydration rate. The numerical challenge is the simplification by homogenization. In this regard, the concrete initial properties are considered the same throughout the structural body but may not be in a structure within site conditions. In addition, the exact location of the sensors in relation to the locations on the numerical model may slightly vary due to the massiveness of the foundation, which contributes to the observed deviations from the recorded true values.
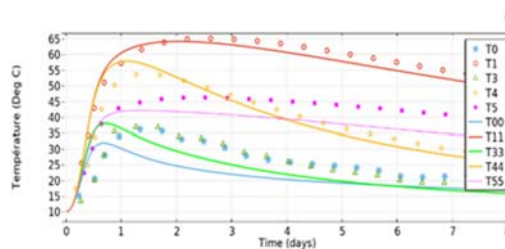
Fig. 7 Evolution of temperature in a wind turbine foundation
* T0-T5 sensor measurements, T00-T55 numerical prediction

The temperature contours within the foundation at the time at which maximum core temperature is experienced is shown on Fig. 8 predicted using the THC model (Fig. 8 (a)) and captured by the fibre optic (Fig. 8 (b)). Upon comparison, similar contours are observed against the same temperature scale where in both figures, a maximum value of about 65 °C at the core is obtained with higher temperature gradients towards the boundaries with air (positions T0 and T3) than that with the soil (position T5) probably due to the higher temperature in the soil than in the air.

Fig. 9 provides the external temperature and humidity evolutions over an 8-day period from the time of casting with an average temperature of 9 °C and average relative humidity of about 95%. Within the time period when pouring took place (t=0 hrs to t=8 hrs), the average external temperature was about 10 °C. With no data on the mixing temperature, the fresh concrete temperature was assumed equal to the external temperature for numerical simulation.

World Academy of Science, Engineering and Technology
International Journal of Civil and Environmental Engineering
Vol:16, No:3, 2022
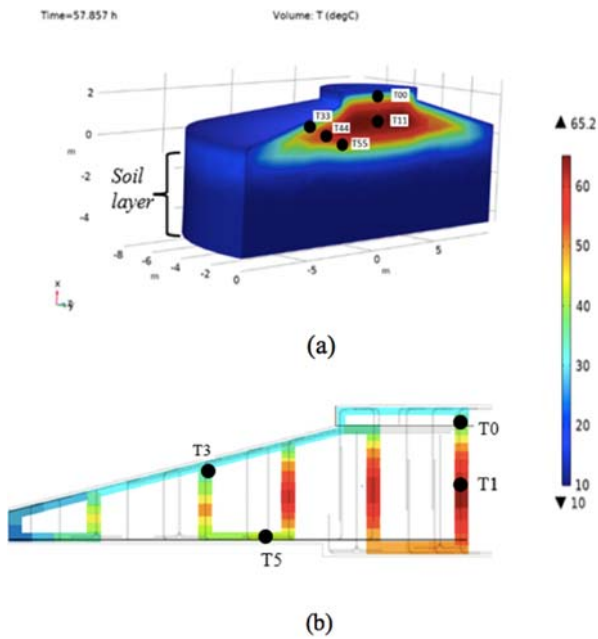
Fig. 8 Foundation's temperature contours at time of maximum core temperature a) Numerical simulation b) Fibre optic measurements
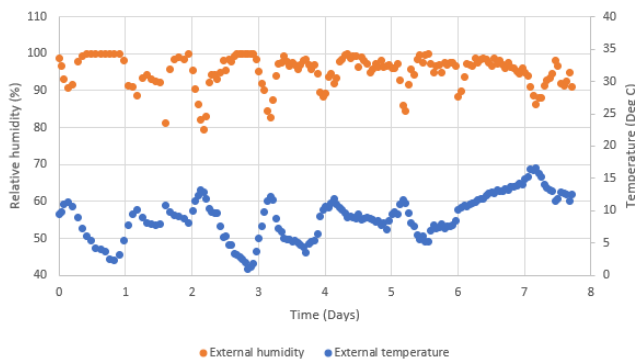
Fig. 9 Evolution of external temperature and relative humidity

In the thermal model, variations of thermal conductivity, external temperature, wind speed and solar radiation with time and the presence of reinforcement bars were not taken into account. In [8], the account for a varying thermal conductivity and capacity with temperature showed a noticeable impact on the maximum temperature. However, as the variation of thermal properties may affect the maximum temperature, [2] reported no change in core temperature with variation in external temperature and solar radiation. The variation was shown to mainly affect the surface temperature.

With regard to account for reinforcement bars, they are modelled using 2D *truss* features provided on COMSOL. They are then physically coupled with the 3D *solid* feature (concrete foundation in this study) at selected points. The deformation of the concrete and the steel at this particular points are considered equal. However, in a thermal analysis, the reinforcements are modelled using 3D *solid* objects (with assigned structural steel thermal properties), but due to the complexity of the reinforcement layout and the quantity, it would be numerically

challenging to model the individual bars in 3D. A study of the effect of percentage of reinforcement bars on maximum temperature using simpler models has been numerically conducted where the reinforcements are modeled using 3D *solid* objects, however, results shall be presented in a subsequent paper.

B. Relative Humidity

The TH coupling (hygro-thermal) allows interdependence of the temperature and relative humidity evolution. Fig. 10 presents a particular trend of the relative humidity evolution whereby it is shown to decrease during temperature increase and a subsequent increase when the temperature drops after attaining its maximum value. This trend is consistent with experimental values provided in [19]. However, results in other research works such as [22] capture a continuous decrease in humidity with increase and decrease in temperature (Fig. 11).
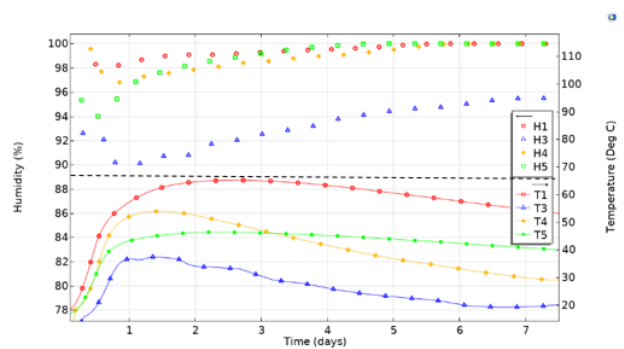
Fig. 10 Relative humidity and temperature evolution on actual foundation
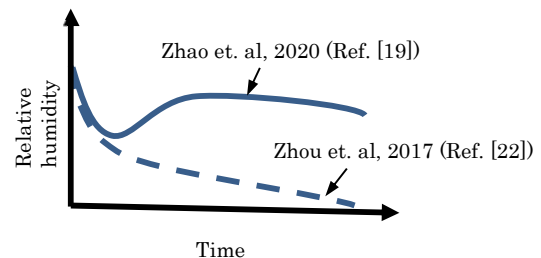
Fig. 11 Humidity evolution in previous studies

The relative humidity evolution in concrete during its hydration is a result of three mechanisms acting simultaneously; 1) thermo-diffusion which is a result of diffusion driven by temperature gradient, 2) moisture diffusion due to mass gradient and 3) change of state from liquid to vapor. The difference between the two trends of relative humidity may be attributed to the three mechanisms acting at varying rates depending on the conditions of the structure being studied.

Furthermore, the spatial variation of the initial measured temperatures relative to the individual maximum temperatures attained is not notable (Fig. 7). This may allow a common initial value to be numerically used in the absence of data. This is not the case for the relative humidity where relatively high variations in initial values can be observed. The hydric portion

World Academy of Science, Engineering and Technology
International Journal of Civil and Environmental Engineering
Vol:16, No:3, 2022

of the THC model therefore needs to be validated through a more controlled environment where the initial humidity can be homogenized and its trend well monitored for interpretation.

IV. Conclusion

In this paper, results from instrumentation of an actual wind turbine are provided and discussed and the formulation of a THC model is also presented. The following points are highlighted.

1. Through the aid of temperature sensors, it is seen that the temperature within wind turbine foundations similar to the one used in the study has potential to achieve high temperatures of about $65\,^{\circ}$C at the core of the foundation. During deconstruction, it would be of interest to obtain core samples to verify presence or absence of ettringite to quantify crack potential.

2. From the sensors placed near the surface and at the core, a temperature difference of $35\,^{\circ}$C is captured. A study on the restraint degree would be necessary for a crack risk analysis.

3. The 3D THC model is seen to well predict the evolutions of temperature within the body of a gravity foundation at five different locations. However, deviations encountered near the surface may be attributed to the use of constant values such as wind speed and external temperature.

4. Numerically, account for effect of reinforcement on the temperature evolution and change in material properties with hydration level would be necessary for more representative results.

References

[1] H. F. W. Taylor, Cement Chemistry, 2 edition, Thomas Telford, London, 1997.

[2] L. Buffo-Lacarrière, A. Sellier, G. Escadeillas, A. Turatsinze, "Multiphasic finite element modeling of concrete hydration," Cement and Concrete Research, Vol. 37, pp. 131–138, 2007.

[3] B., Kolani, L., Buffo-Lacarrière, A., Sellier, G., Escadeillas, L., Boutillon, L., Linger, "Hydration of slag-blended cements," Cement & Concrete Composites, Vol. 34, pp. 1009–1018, 2012.

[4] G. De Schutter, L. Taerwe, "General hydration model for Portland cement and blast furnace slag cement," Cement and Concrete Research, Vol. 25, pp. 593–604, 1995.

[5] F. J. Ulm, O. Coussy, "Modeling of thermo-chemo-mechanical couplings of concrete at early ages," J. Eng. Mech. – ASCE Vol. 121, pp. 785–794, 1995.

[6] O. Coussy, "Poromechanics, " John Wiley & Sons, Ltd, Chichester, UK, 2005.

[7] ACI Committee No. 301-10, Specifications for Structural Concrete: An ACI Standard, American concrete Institute, 2010.

[8] M. Briffaut , F. Benboudjema , J. M. Torrenti & G. Nahas (2012), "Effects of early-age thermal behaviour on damage risks in massive concrete structures, " European Journal of Environmental and Civil Engineering, Vol. 16, pp. 589-605.

[9] Z. P. Bazant, L. J. Najjar, Nonlinear water diffusion in nonsaturated concrete, Mater. Struct. 5 (1972) 3–20.

[10] M. Wyrzykowski, P. Lura, Effect of relative humidity decrease due to self-desiccation on the hydration kinetics of cement, Cem. Concr. Res. 85 (2016) 75–81.

[11] M. Collepardi, "A state-of-the-art review on delayed ettringite attack on concrete," Cement & Concrete Composites, Vol.25, pp, 401–407, 2003.

[12] L. Lacarriere, et al, "Restrained shrinkage of massive reinforced concrete structures: results of the project CEOS.fr," European Journal of Environmental and Civil Engineering, Taylor & Francis, Vol. 20, pp.785-808, 2016.

[13] J. Xin, G. Zhang, Y. Liu, Z. Wang, Z. Wu, "Effect of temperature history and restraint degree on cracking behavior of early-age concrete," Construction and Building Materials, Vol. 192, pp. 381-390, 2018.

[14] M. Cervera, J. Oliver, T. Prato, "Thermo-chemo-mechanical model for concrete. I: Hydration and aging," J. Eng. Mech. – ASCE Vol. 125, pp. 1018–1027, 1999.

[15] D. Gawin, F. Pesavento, B.A. Schrefler, "Hygro-thermo-chemo-mechanical modeling of concrete at early ages and beyond. Part I: hydration and hygro-thermal phenomena," Int. J. Numer. Meth. Eng. Vol. 67, pp. 299–331, 2006.

[16] G. Di Luzio, G. Cusatis, "Hygro-thermo-chemical modeling of high performance concrete. I: Theory," Cement and Concrete Composites, Vol. 31, pp. 301–308, 2009.

[17] COMSOL Multiphysics version 5.2a, COMSOL AB, Stockholm, Sweden, 2016.

[18] M. Y. Du, X. Y. Jin, H. L. Ye, et al., "A coupled hygro-thermal model of early-age concrete based on micro-pore structure evolution," Construction and Building Material, Vol. 111, pp. 689–698, 2016.

[19] H. Zhao, K. Jiang, R. Yang, Y. Tange, J. Liu, "Experimental and theoretical analysis on coupled effect of hydration, temperature and humidity in early-age cement-based materials," International Journal of Heat and Mass Transfer. Vol. 146, 2020.

[20] V. Baroghel-Bouny, M. Mainguy, T. Lassabatere, O. Coussy, "Characterization and identification of equilibrium and transfer moisture properties for ordinary and high performance cementitious materials," Cement and Concrete Research, Vol. 29, pp. 1225–1238, 1999.

[21] K. Maekawa, T. Ishida, T. Kishi, "Multi-scale Modeling of Structural Concrete," Taylor and Francis, 2009.

[22] W. Zhou, T. Q. Qi, X. H. Liu, et al., A hygro-thermo-chemical analysis of concrete at an early age and beyond under dry-wet conditions based on a fixed model, Int. J. Heat Mass Transf. 115 (2017) 488–499.